Electronic Supplementary Information

Carbamoylmannose Enhances Tumor Targeting of Supramolecular Nanoparticles Formed through Host-Guest Complexation of a Pair of Homopolymers

Xikuang Yao,[a] Qiwen Zhu,[b] Cheng Li,[a] Kangjun Yuan,[a] Rui Che,[b] Peng Zhang,[a] Chenchen Yang,[a] Wei Lu,*[b] Wei Wu,[a] Xiqun Jiang,*[a]

[a] Department of Polymer Science & Engineering, College of Chemistry & Chemical Engineering, Nanjing University, Nanjing 210093, P. R. China

[b] School of Chemistry and Molecular Engineering, East China Normal University, 3663 North Zhongshan Road, Shanghai 200062, P. R. China

* To whom correspondence should be addressed

Tel/Fax: 86 25 89687138

Email: jiangx@nju.edu.cn, wlu@chem.ecnu.edu.cn

3-O-carbamoyl-2-propynyl-2,4,6-tris-O-acetyl-α-D-mannopyranoside

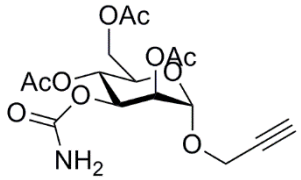

Into a solution of 1,2,4,6-textra-O-acetyl-3-O-carbamoyl-α-D-mannopyranoside (1.5 g, 3.8 mmol) and propargyl alcohol (1.15 mL, 19.2 mmol) in 20mL of anhydrous DCM was added $BF_3{\cdot}Et_2O$ (4.74 mL, 38.4 mmol) dropwise at 0 °C under nitrogen. The mixture was stirring at 0-20 °Cfor 24 h. The reaction was quenched with saturated aqueous $NaHCO_3$ at 0 °C, and the mixture was extracted with DCM. The organic layer was washed subsequently with water, saturated aqueous Na_2CO_3, and brine, dried by Na_2SO_4 and concentrated. The crude product was purified by silica gel column chromatography (EtOAc/petroleum ether 2:1) to yield 3-O-carbamoyl-2-propynyl-2,4,6-tris-O-acetyl-α-D-mannopyranoside as a white solid (0.74g, 50.2%). $[\alpha]_D^{25}$+56 (0.1, $CHCl_3$), m.p. 110.5-112.5 °C (Optical rotations were measures at 25°C using a Rudolph Autopol VI.). ^1H and ^{13}C spectra were recorded on a Bruker Ascend400 (400 MHz and 100 MHz). High-resolution mass spectral analyses were run on a microTOF 10293.

^1H NMR (400 MHz, $CDCl_3$) δ 5.35 – 5.20 (m, 3H), 5.05 (s, 1H), 4.85 (s, 2H), 4.29 (dd, *J* = 14.1, 3.7 Hz, 3H), 4.11 (dd, *J* = 12.3, 2.2 Hz, 1H), 4.06 – 4.00 (m, 1H), 2.49 (t, *J* = 2.2 Hz, 1H), 2.16 (s, 3H), 2.11 (s, 3H), 2.07 (s, 3H);

^{13}C NMR (101 MHz, $CDCl_3$) δ 170.66, 169.94, 169.92, 155.27, 96.26, 77.98, 77.38, 77.06, 76.75, 75.59, 69.85, 69.01, 66.16, 62.35, 55.01, 20.91, 20.75;

HR-MS *m/z*: 410.1058, (calculated for $C_{16}H_{21}NNaO_{10}$, 410.1058).

2-propynyl-3-O-carbamoyl-D-mannose (PCM)

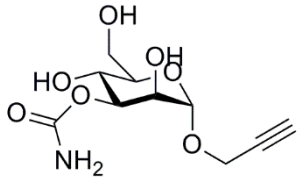

To a cooled (0 °C) solution of 3-O-carbamoyl-2-propynyl-2,4,6-tris-O-acetyl-α-D-mannopyranoside (584mg, 1.5mmol) in 12mL of anhydrous MeOH was added K_2CO_3 (30mg, 0.2mmol) in potion. The mixture was reacted at 0 °C for 3 h. The solution was then neutralized by addition of iron-exchange resin until pH 7, filtered and concentrated. The crude product was purified by silica gel column chromatography (0% - 5% MeOH: CH_2Cl_2) to yield PCM as a white solid (340mg, 86.5%). $[\alpha]_D^{25}$+79 (0.122, MeOH), m.p. 146-148 °C.

^1H NMR (400 MHz, MeOD) δ 4.99 (s, 1H), 4.83 (dd, *J* = 9.9, 3.2 Hz, 1H), 4.31 (d, *J* = 2.2 Hz, 2H), 4.00 (s, 1H), 3.91 – 3.80 (m, 2H), 3.74 (dd, *J* = 11.7, 5.7 Hz, 1H), 3.66 – 3.58 (m, 1H), 2.88 (d, *J* = 2.2 Hz, 1H).

^{13}C NMR (101 MHz, MeOD) δ159.37, 99.74, 79.89, 76.14, 75.90, 75.28, 70.15, 65.97, 62.64, 54.90, 49.67, 49.45, 49.24, 49.03, 48.82, 48.60, 48.39.

HR-MS *m/z*: 284.0728, (calculated for $C_{10}H_{15}NNaO_7$, 284.0741).

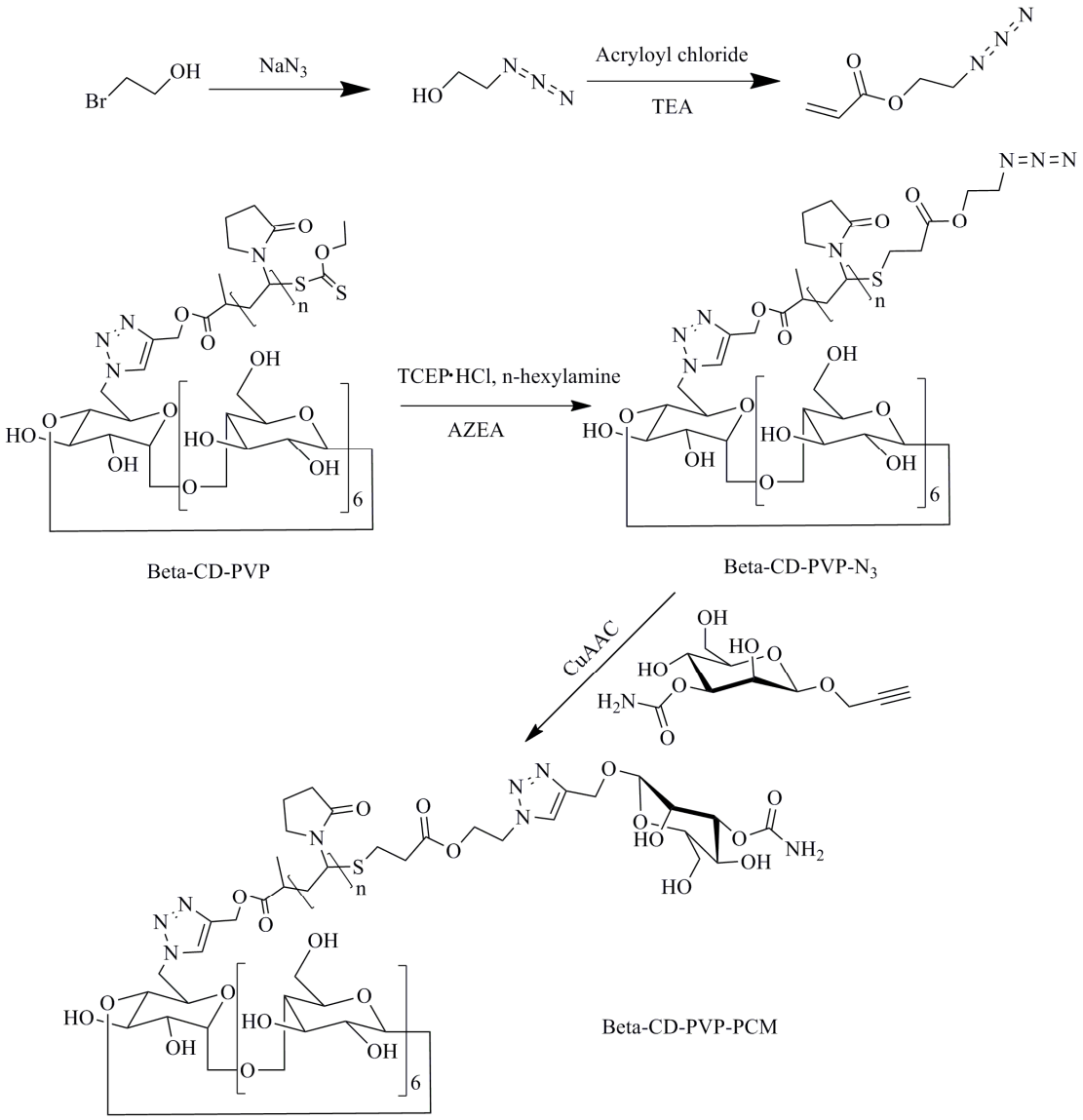

Scheme S1. The synthesis route of β-CD-PVP-PCM.

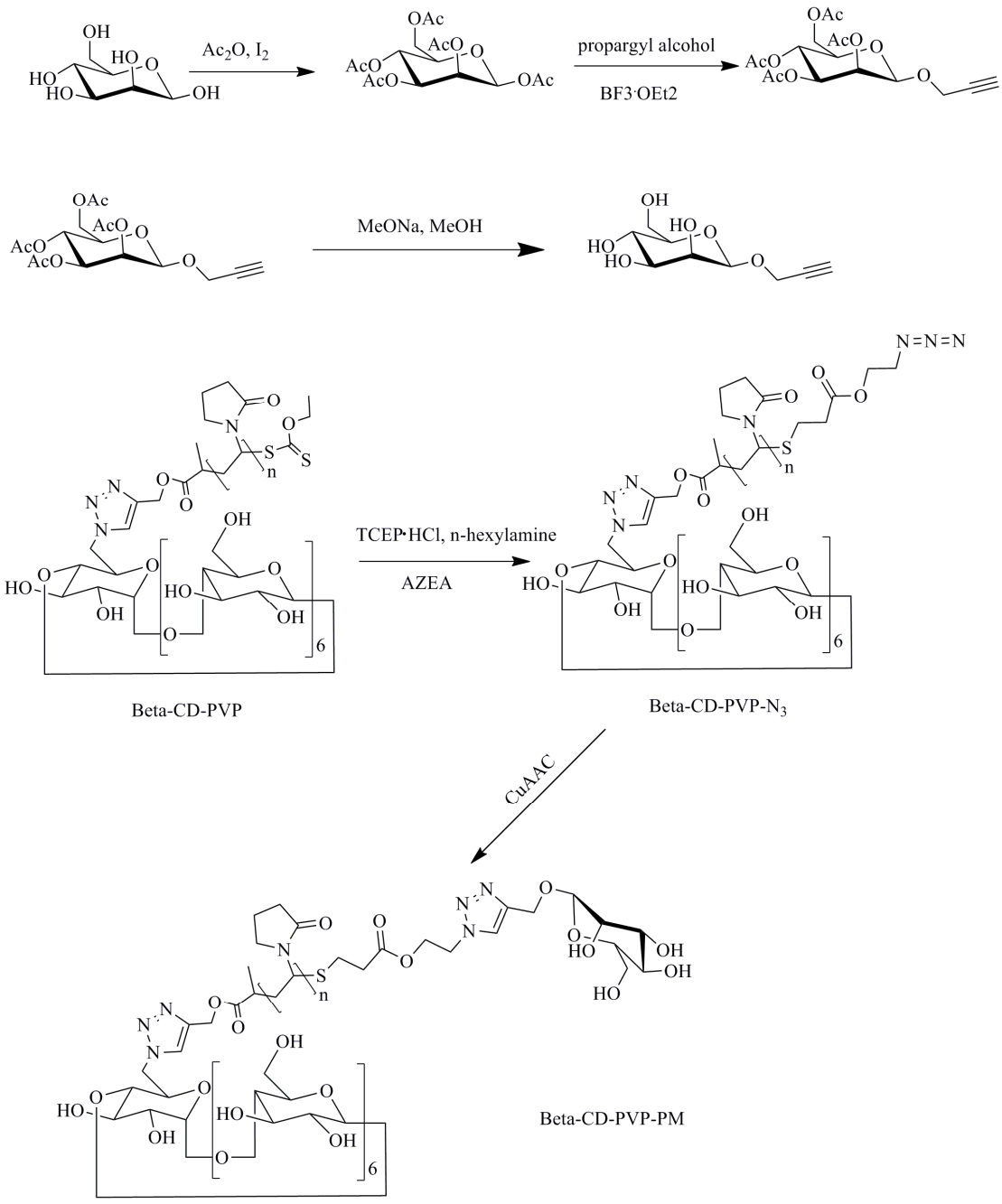

Scheme S2. The synthesis route of β-CD-PVP-PM.

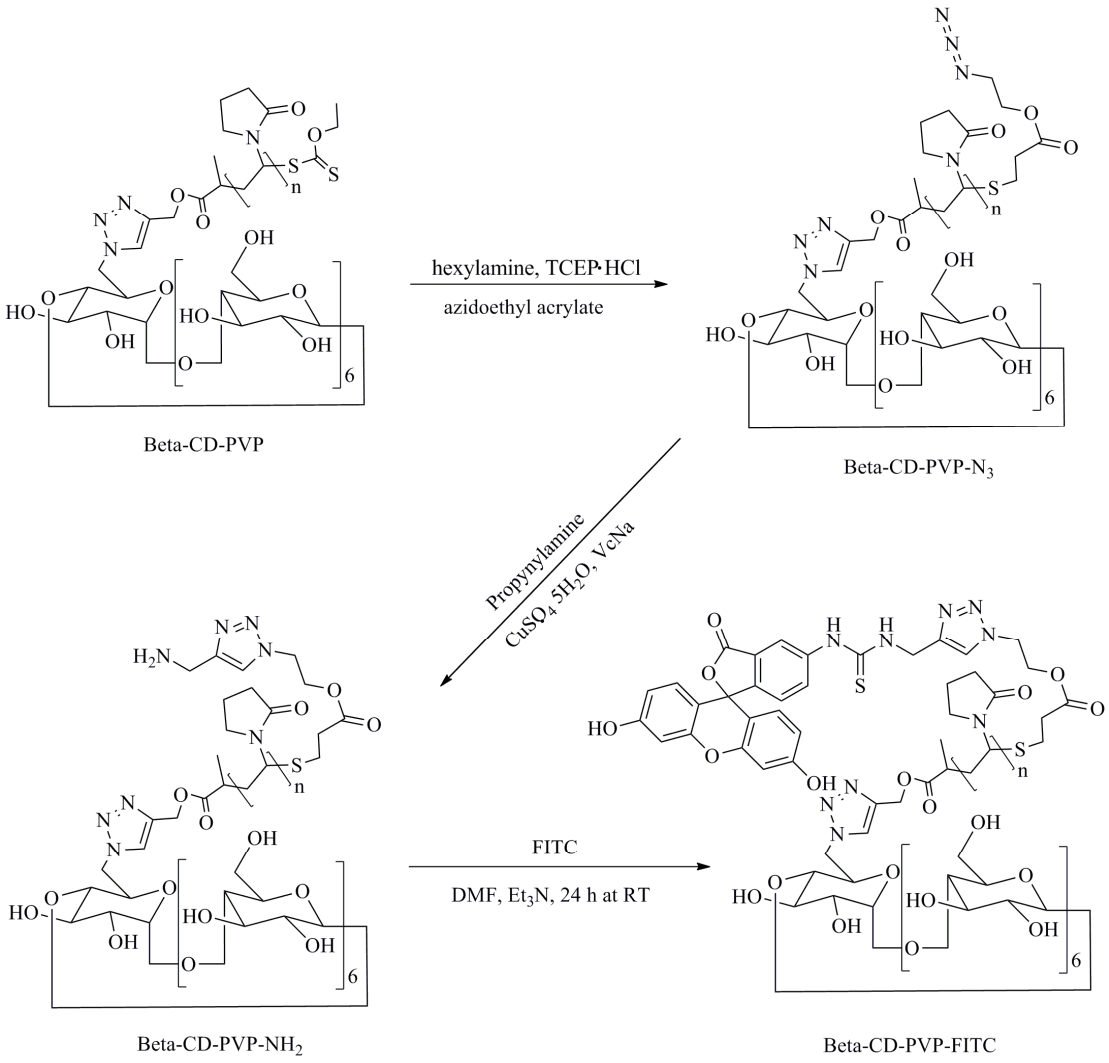

Scheme S3. The synthesis route of FITC-labeled β-CD-PVP.

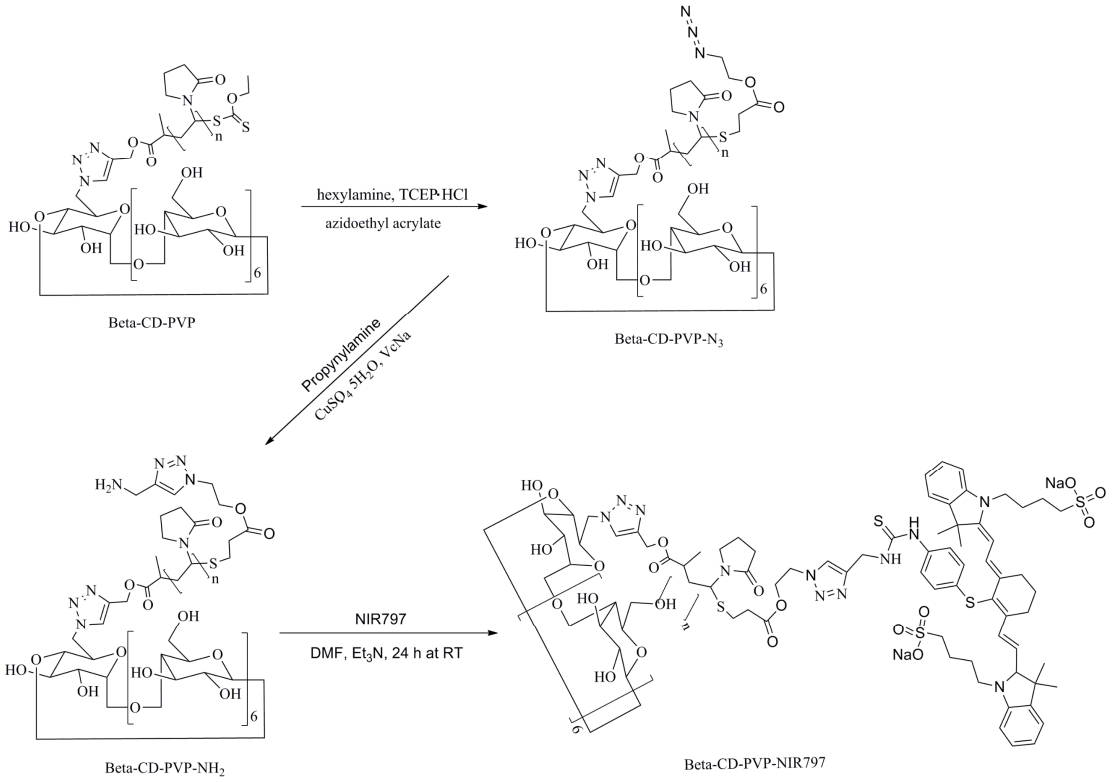

Scheme S4. The synthesis route of NIR797-labeled β-CD-PVP.

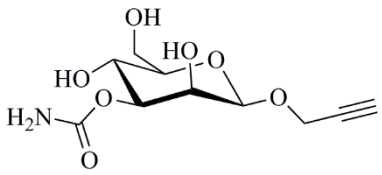

2-propargyl-3-O-carbamoyl-D-mannose (PCM)

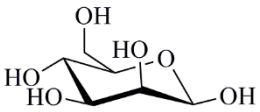

D-mannose

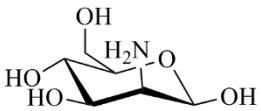

D-mannosamine (MA)

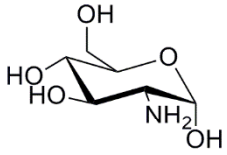

D-glucosamine (GA)

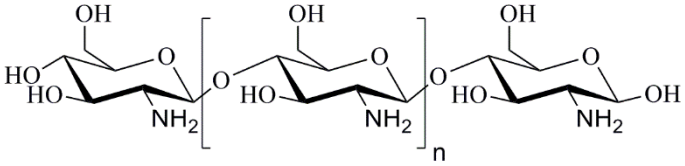

Chitosan

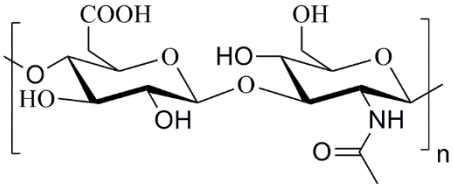

Hyaluronic Acid (HA)

Scheme S5. The structure of used various monosaccharides and polysaccharides.

Table S1. The characteristics of these platinum-incorporating nanoparticles.

No.	Formation	Diameter (nm)	PDI	Zeta-potential (mv)	Drug Loading Content (DLC)	Drug Encapsulation Efficiency (DEE)
1	PVPA-Pt NPs	65	0.16	-13.11 ± 2.31	39%	52%
2	PM-PVPA-Pt NPs	63	0.19	-15.46 ± 1.75	42%	56%
3	PCM-PVPA-Pt NPs	66	0.18	-14.15 ± 3.21	41%	55%

Table S2. The IC_{50} values of different formations after incubated with three various cancer cells for 48 h.

No.	Cells	IC_{50} (μg/mL)			
		Free CDDP	PVPA-Pt NPs	PM-PVPA-Pt NPs	PCM-PVPA-Pt NPs
1	A549	25.1	50.1	46.8	40.7
2	SH-SY5Y	26.9	37.2	36.3	32.4
3	H22	1.9	30.9	17.0	12.0

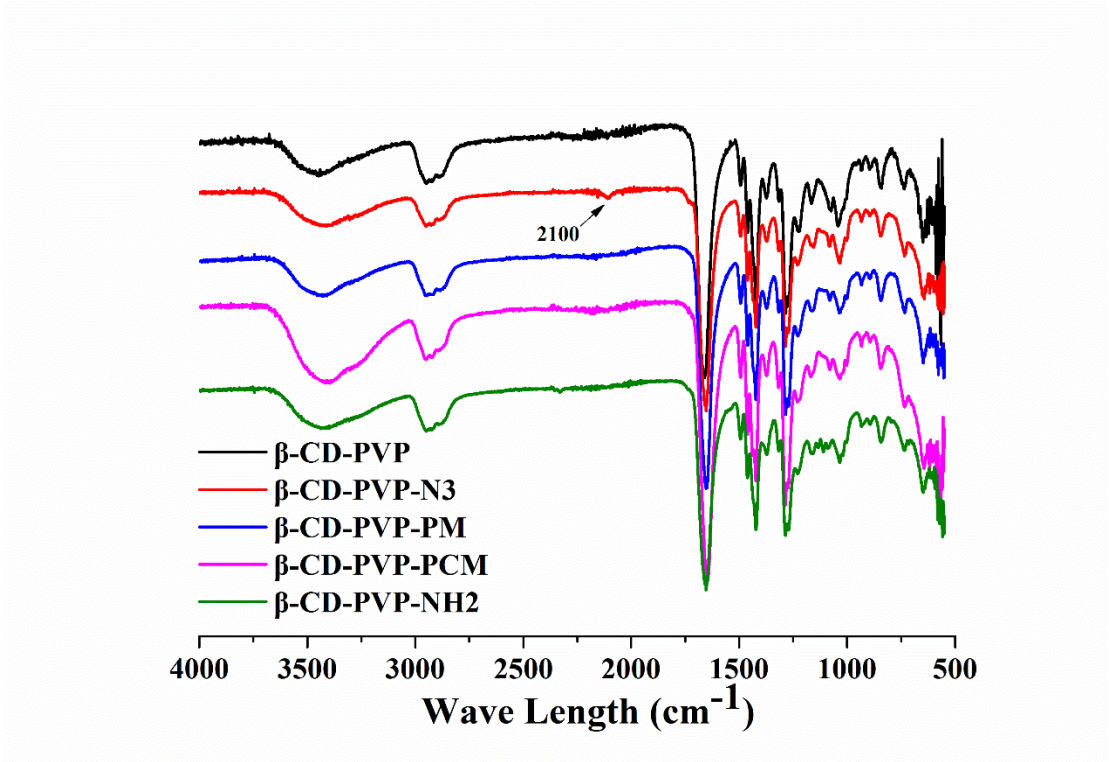

Figure S1. The FT-IR spectra of various β-CD-PVP polymers.

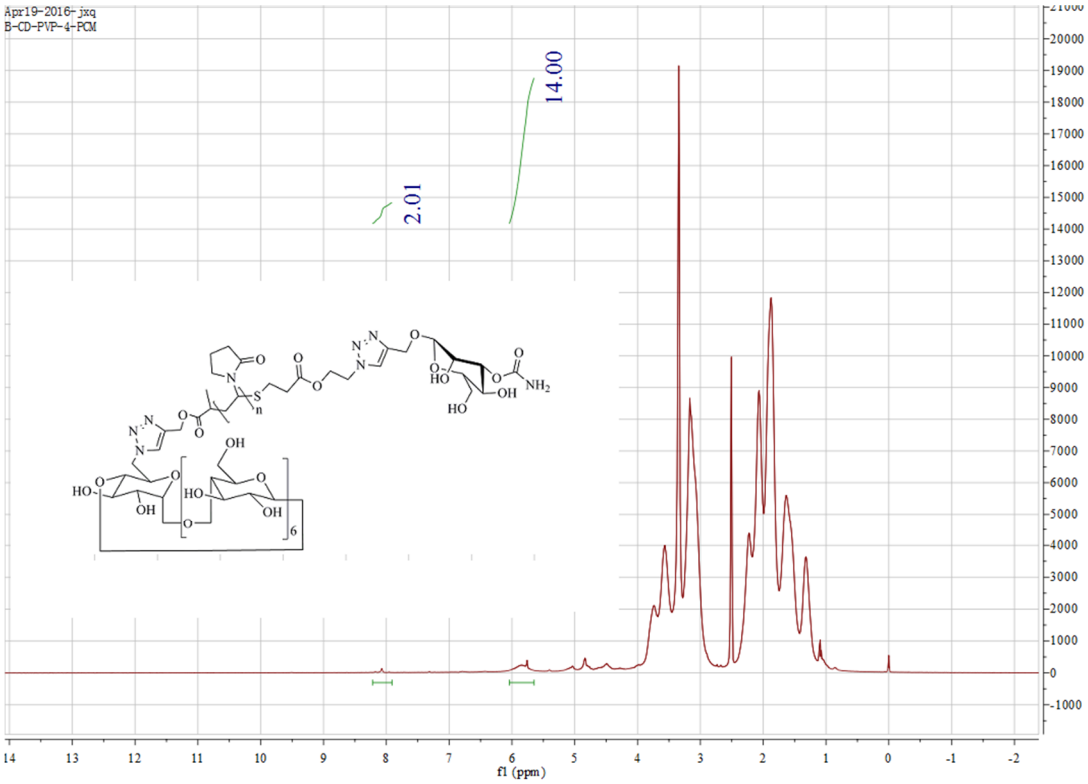

Figure S2. The ^{1}H NMR spectrum of β-CD-PVP-PCM (solvent: DMSO-d_6).

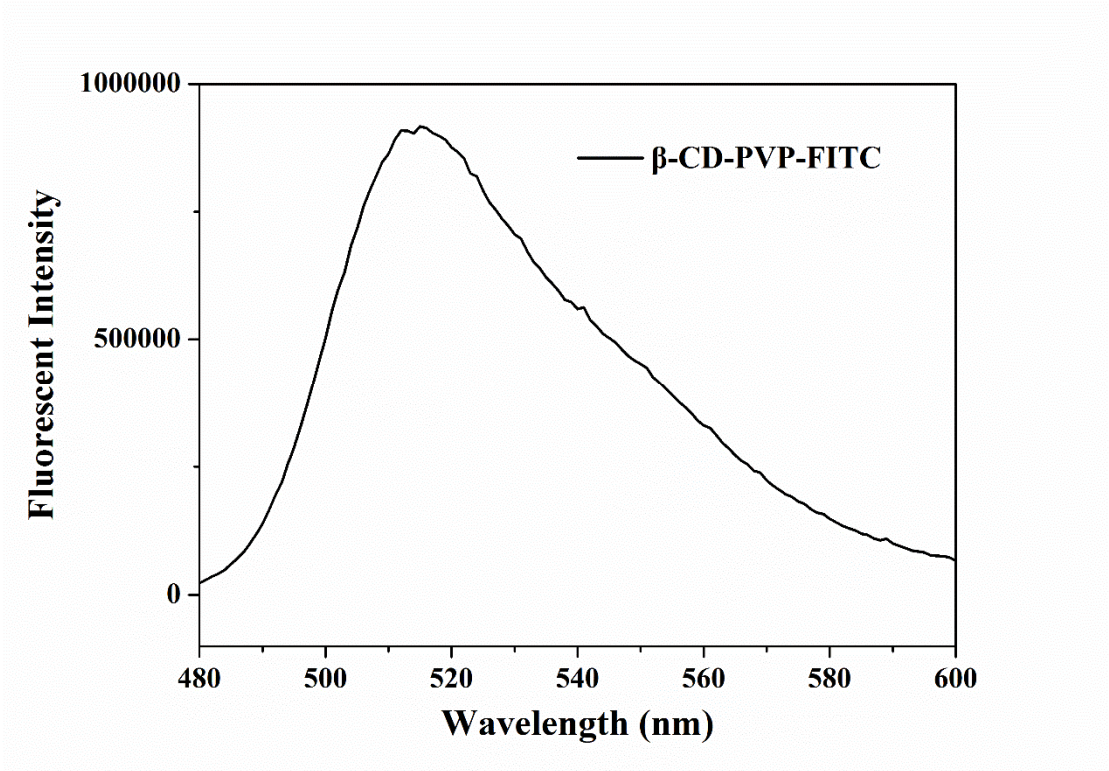

Figure S3. The fluorescent spectrum of β-CD-PVP-FITC. Excitation: 450 nm.

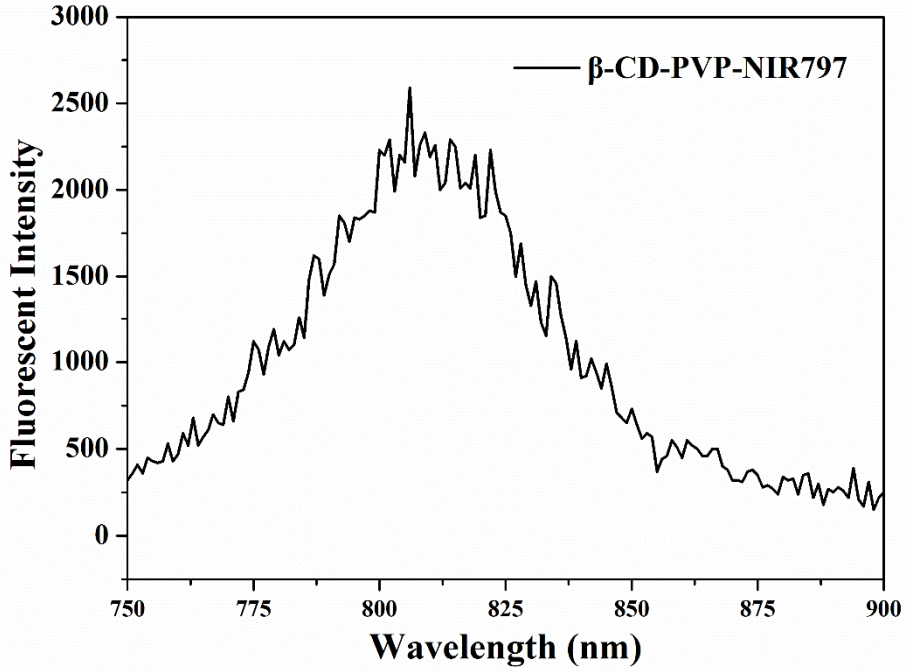

Figure S4. The fluorescent spectrum of β-CD-PVP-NIR797. Excitation: 704 nm.

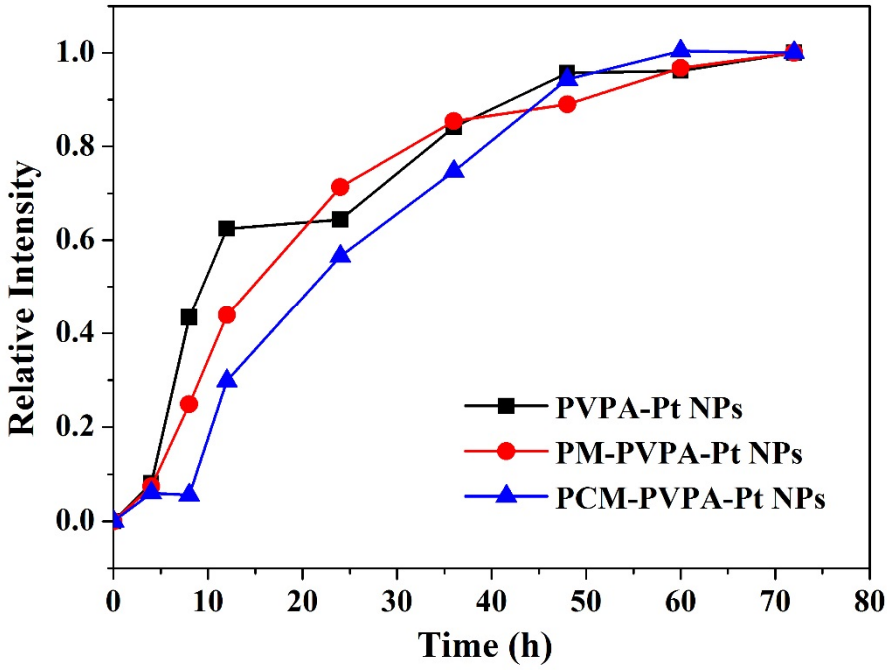

Figure S5. The relative DLS intensity curves of these platinum-incorporating nanoparticles during the preparation.

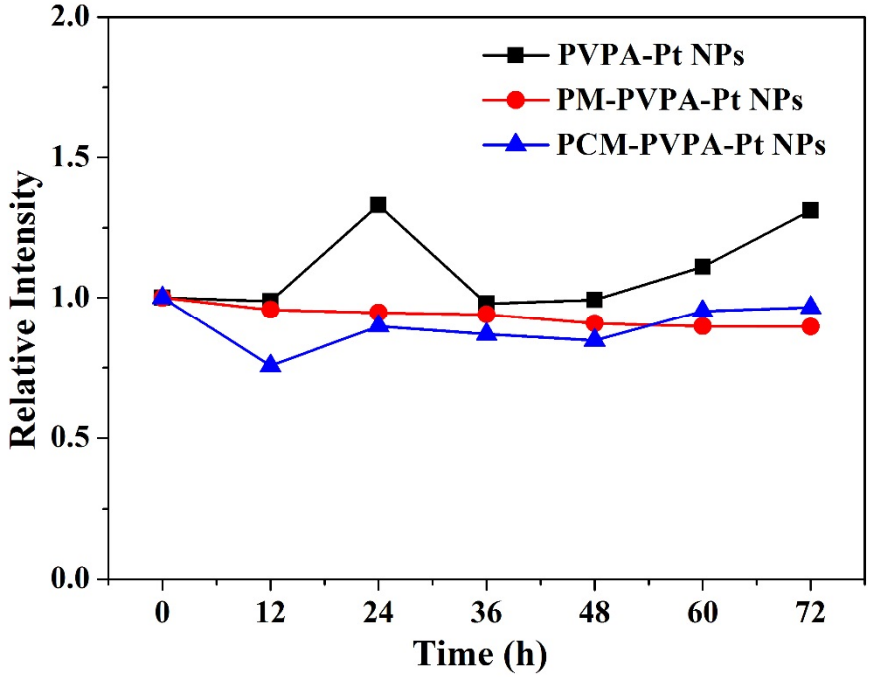

Figure S6. The relative DLS intensity of these platinum-incorporating nanoparticles in deionized water at 37 °C.

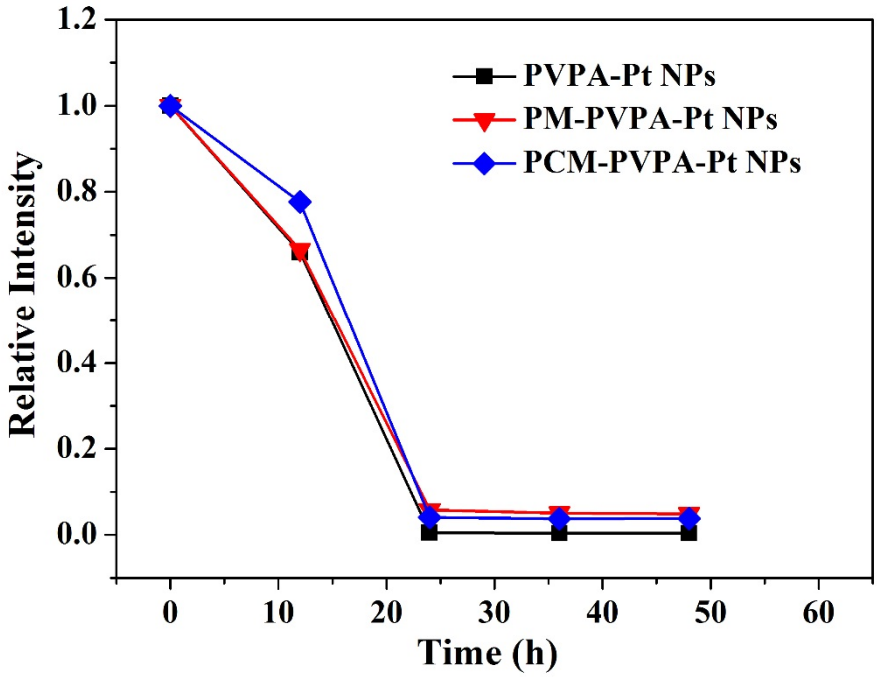

Figure S7. The dissociation behaviours of these platinum-incorporating nanoparticles in 10 mM PBS containing 150 mM NaCl.

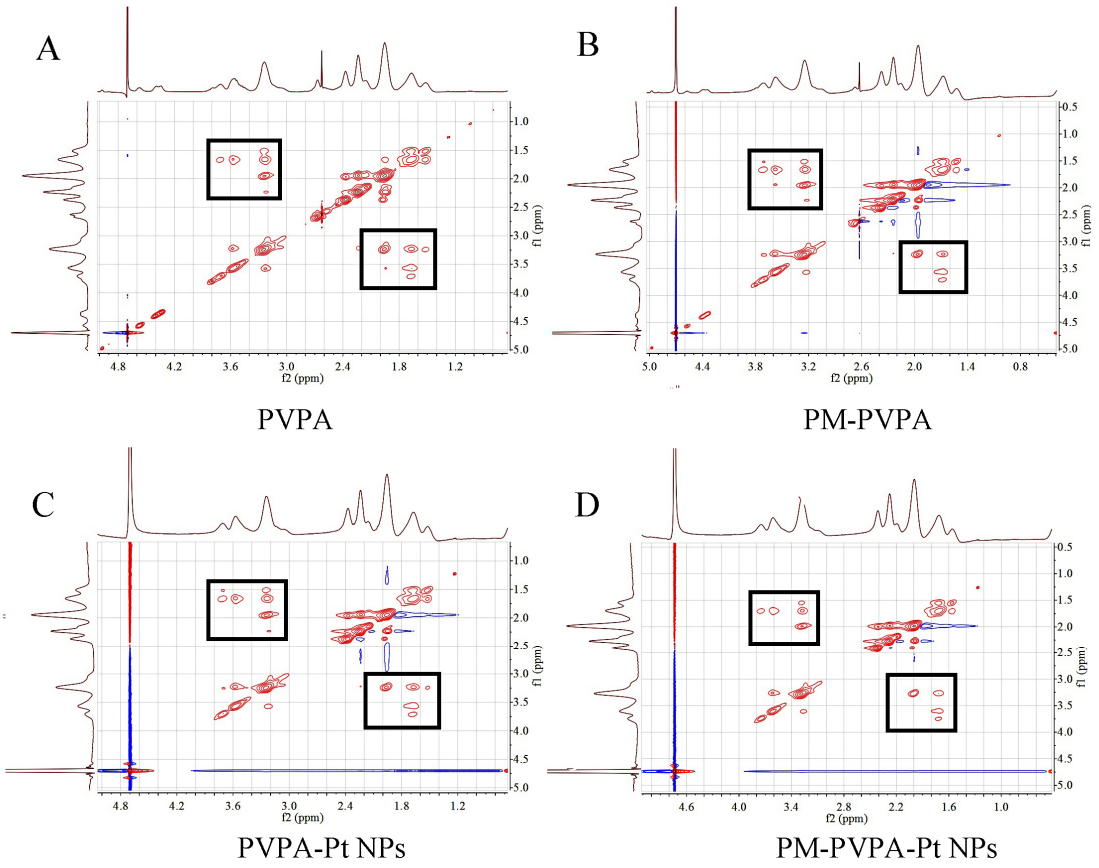

Figure S8. The 2D NOESY spectra of PVPA (A), PM-PVAP (B), PVPA-Pt NPs (C), and PM-PVPA-Pt NPs (D), respectively (solvent: D_2O).

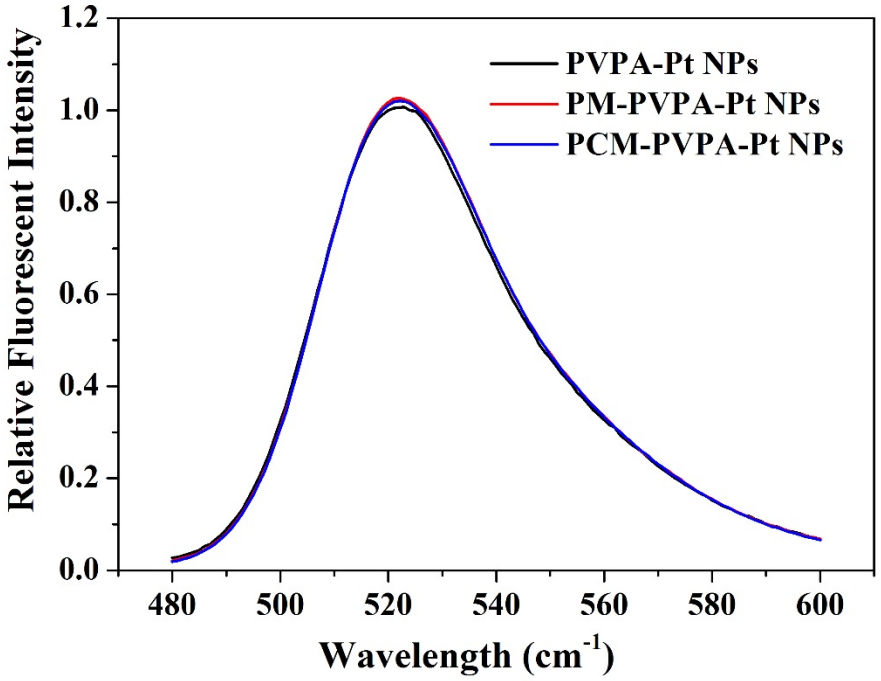

Figure S9. The relative FITC fluorescent intensity of these platinum-incorporating nanoparticles. Excitation: 450 nm.

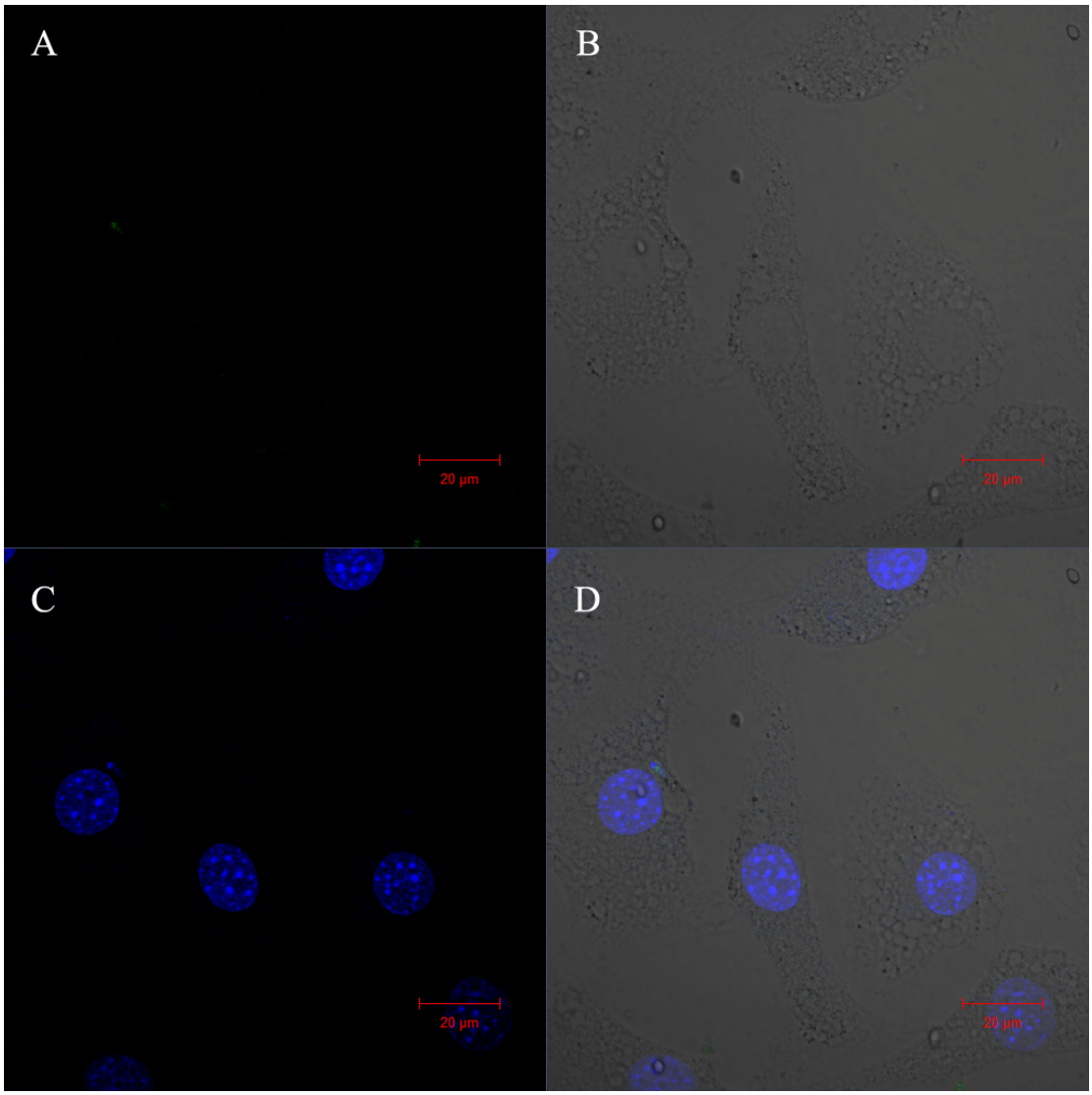

Figure S10. The CLSM images of NIH3T3 cells after incubated with FITC-labeled PCM-PVPA-Pt NPs at 37 ^{o}C for 4 h. (A) is the FITC channel, (B) is the bright field, (C) is the Hoechst 33258 channel, and (D) is the merged image.

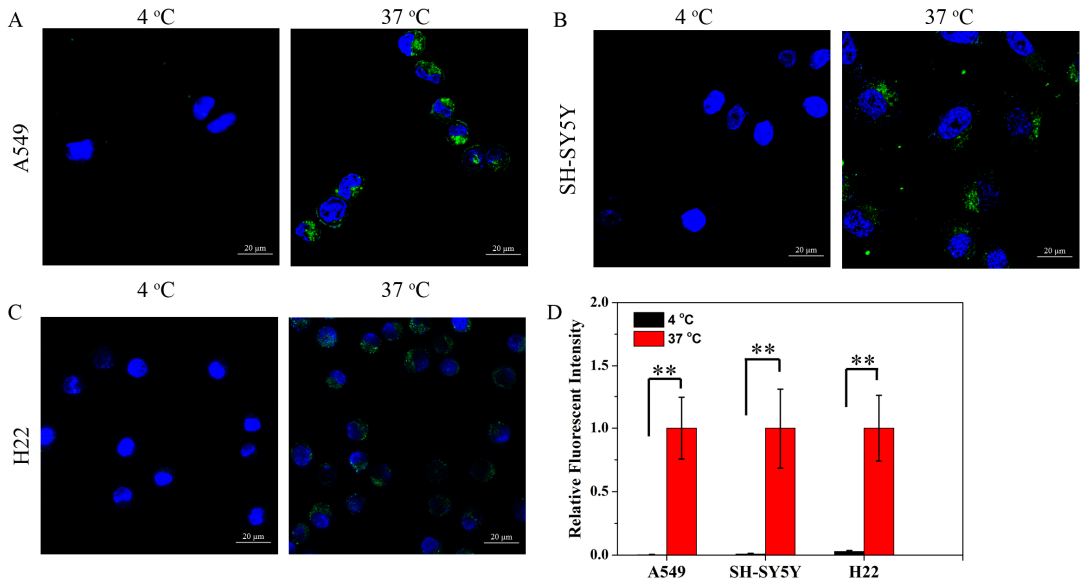

Figure S11. The CLSM images of A549 cells (A), SH-SY5Y cells (B) and H22 cells (C) after treated with PCM-PVPA-Pt NPs at 4 °C or 37 °C for 4 h. (D) Quantitative data for the relative fluorescent intensity. (n = 10 in at least three different CLSM images, ** represents $P < 0.01$)

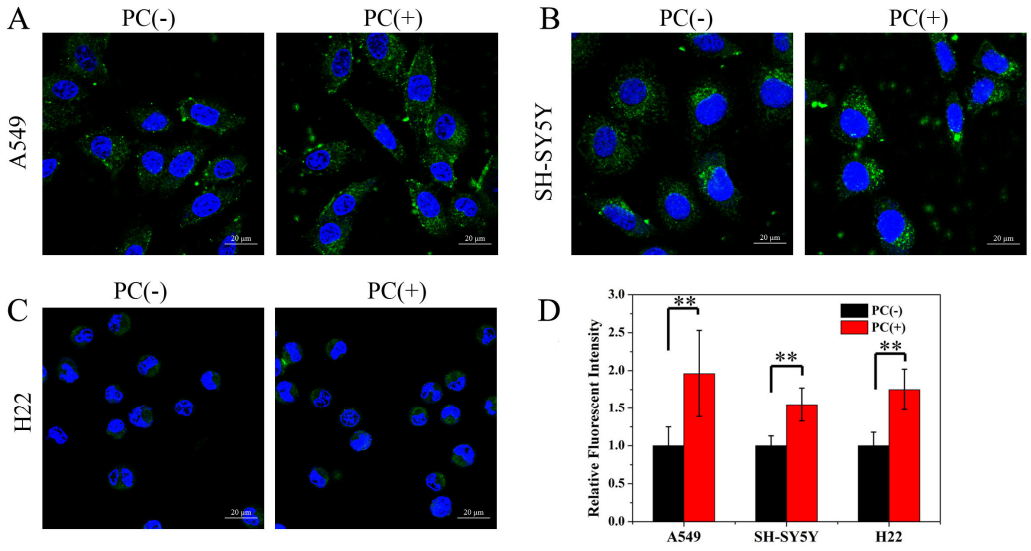

Figure S12. The CLSM images of A549 cells (A), SH-SY5Y cells (B) and H22 cells (C) after treated with PCM-PVPA-Pt NPs in the absence (-) or presence (+) of 3 μM phosphocreatine (PC) at 37 °C for 4 h. (D) Quantitative data for the relative fluorescent intensity. (n = 10 in at least three different CLSM images, ** represents $P < 0.01$)

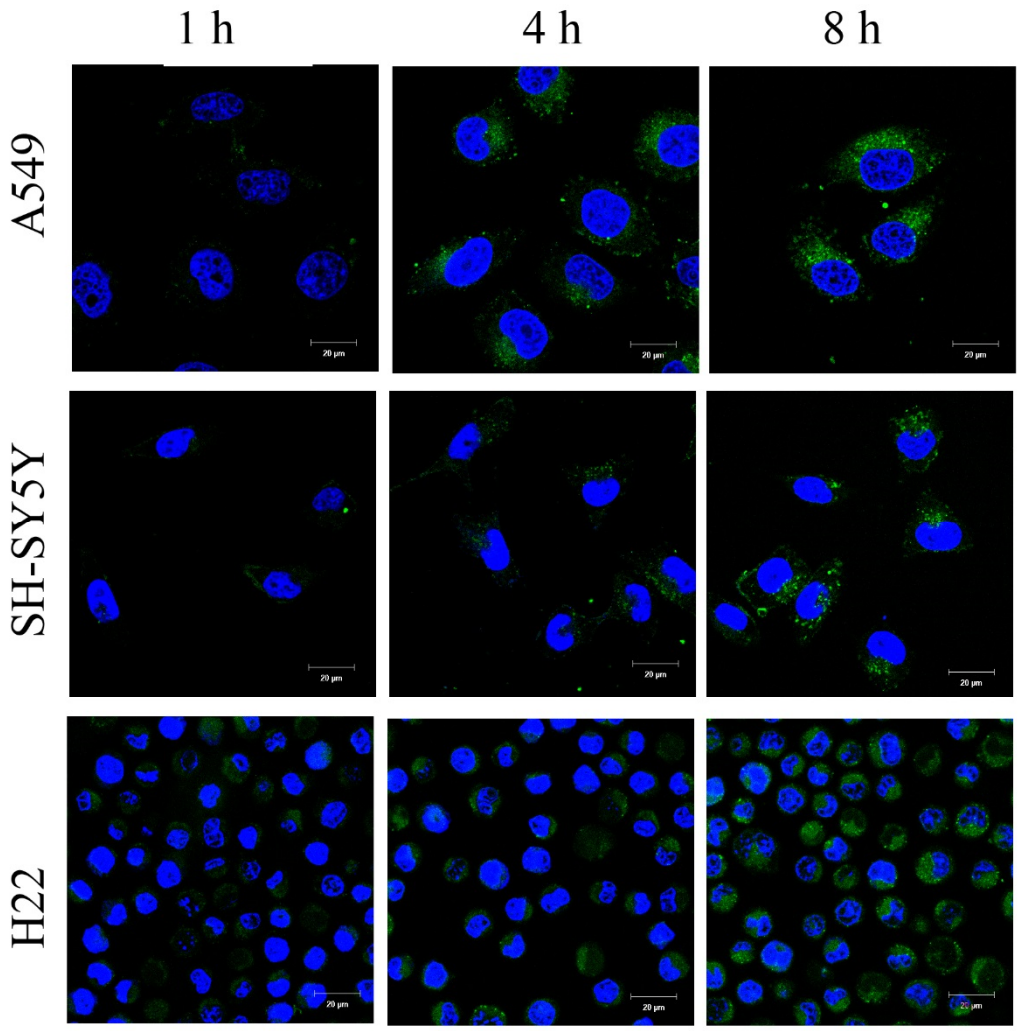

Figure S13. The CLSM images of A549 cells, SH-SY5Y cells and H22 cells after treated with FITC-labeled PCM-PVPA-Pt NPs at 37 ^{o}C for different time.

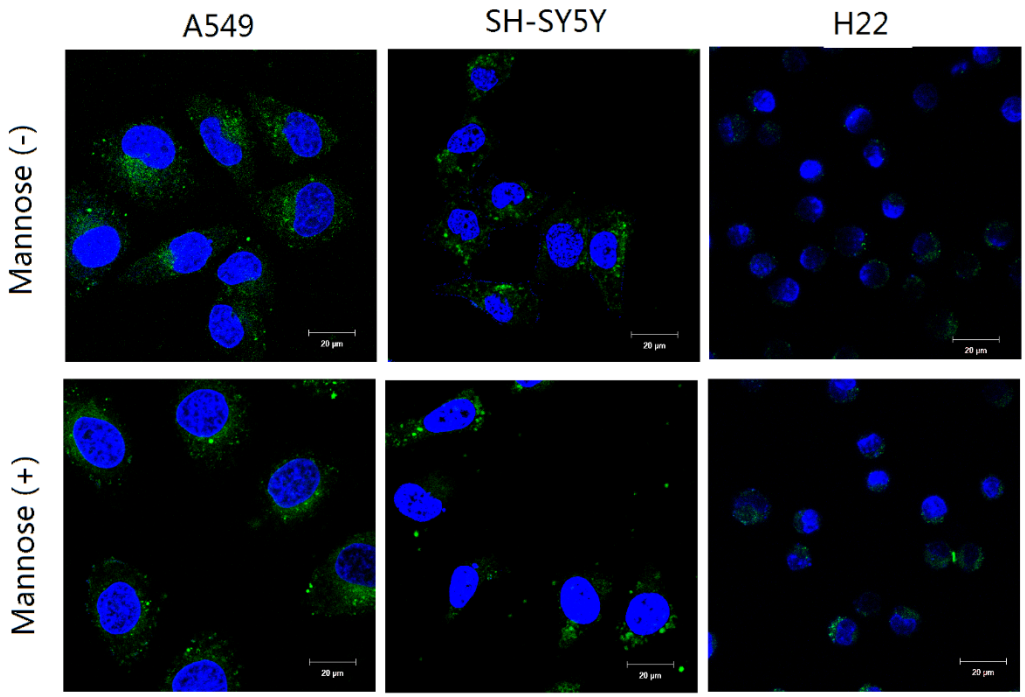

Figure S14. The CLSM images of A549 cells, SH-SY5Y cells and H22 cells after treated with FITC-labeled PCM-PVPA-Pt NPs at 37 ^{o}C for 4 h in the absence (-) or presence (+) of 600 μM Mannose.

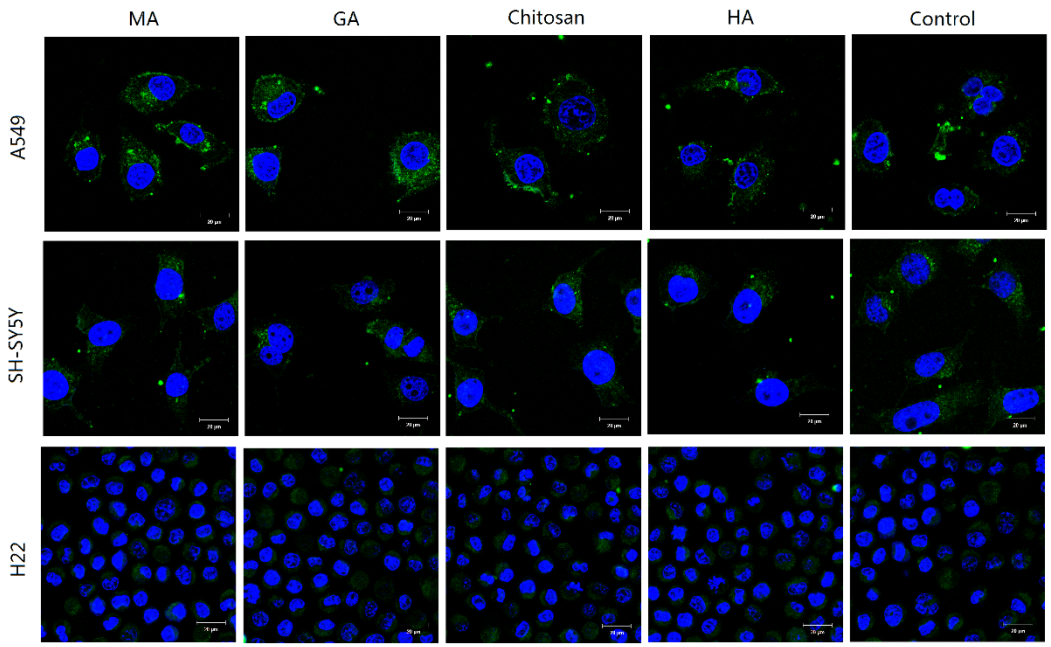

Figure S15. The CLSM images of A549 cells, SH-SY5Y cells and H22 cells after treated with FITC-labeled PCM-PVPA-Pt NPs at 37 ^{o}C for 4 h in the presence of D-mannosamine (MA), D-glucosamine (GA), chitosan, and hyaluronic acid (HA).

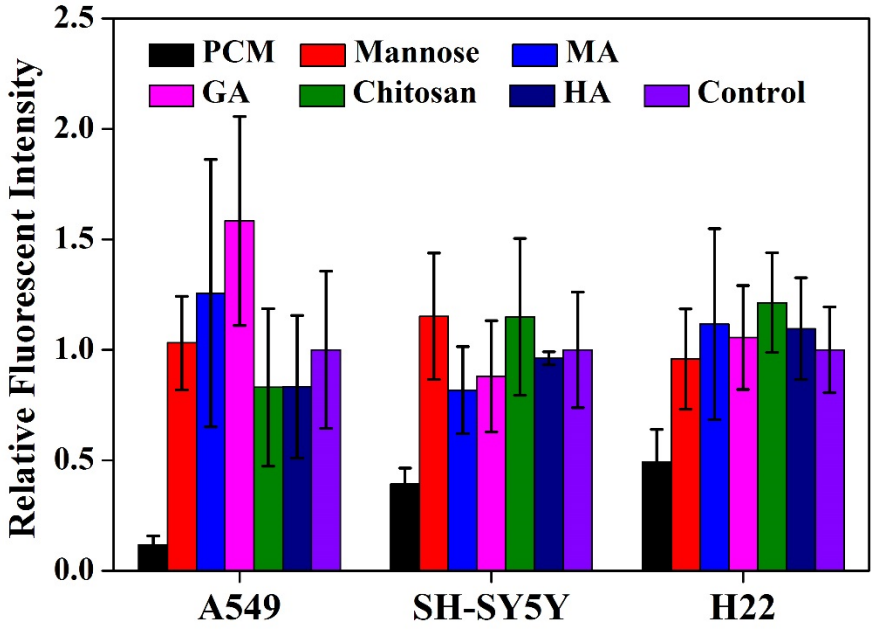

Figure S16. The quantification of fluorescent intensity in A549 cells, SH-SY5Y cells and H22 cells after incubated with FITC-labeled PCM-PVPA-Pt NPs at 37 ^{o}C for 4 h in the presence of various saccharides.

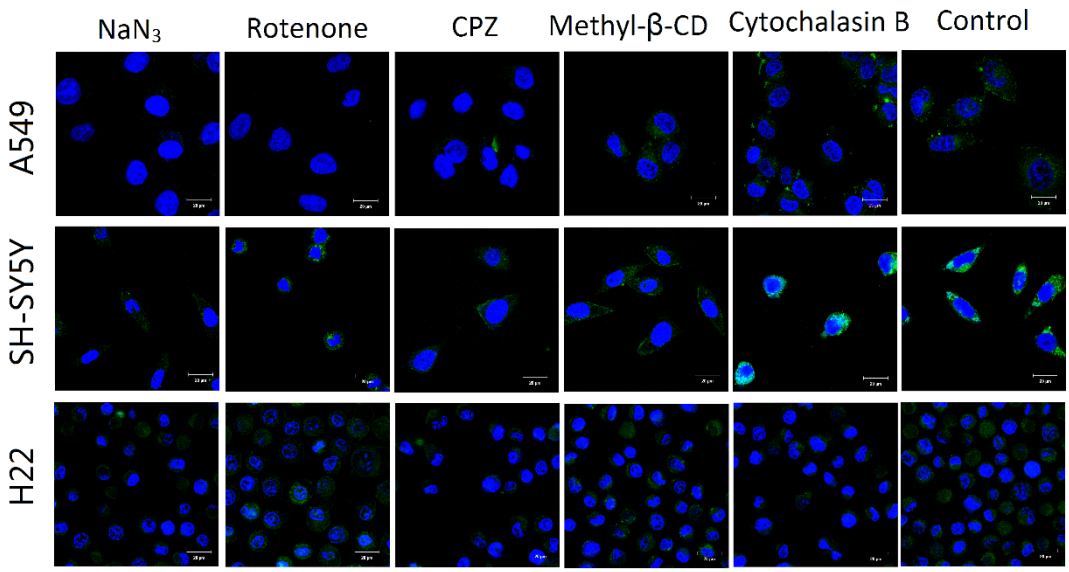

Figure S17. The CLSM images of A549 cells, SH-SY5Y cells and H22 cells after incubated with FITC-labeled PCM-PVPA-Pt NPs at 37 °C for 4 h in the presence of various endocytosis inhibitors.

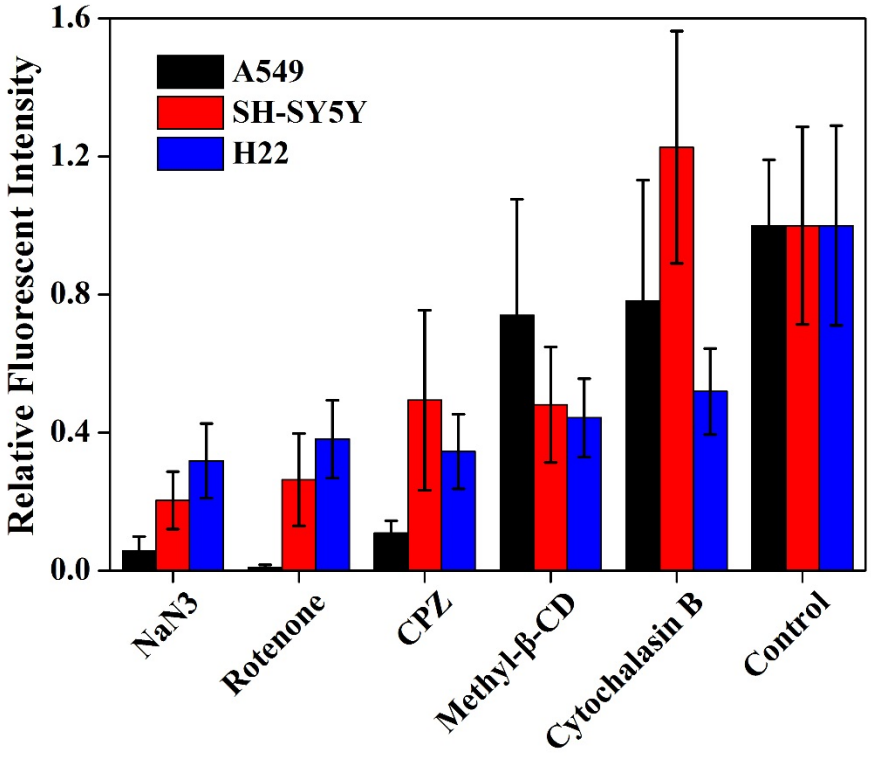

Figure S18. The quantification of fluorescent intensity in A549 cells, SH-SY5Y cells and H22 cells after incubated with FITC-labeled PCM-PVPA-Pt NPs at 37 ^{o}C for 4 h in the presence of various endocytosis inhibitors.

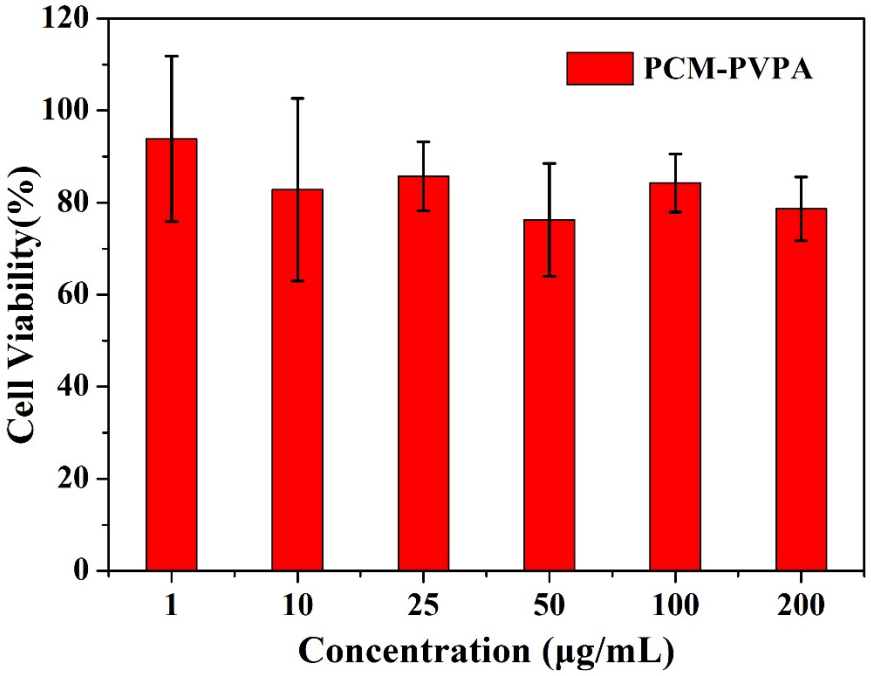

Figure S19. The *in vitro* A549 cell viability after treated with PCM-PVAP pseudo block polymer at 37 ^{o}C for 48 h on different polymer concentration.

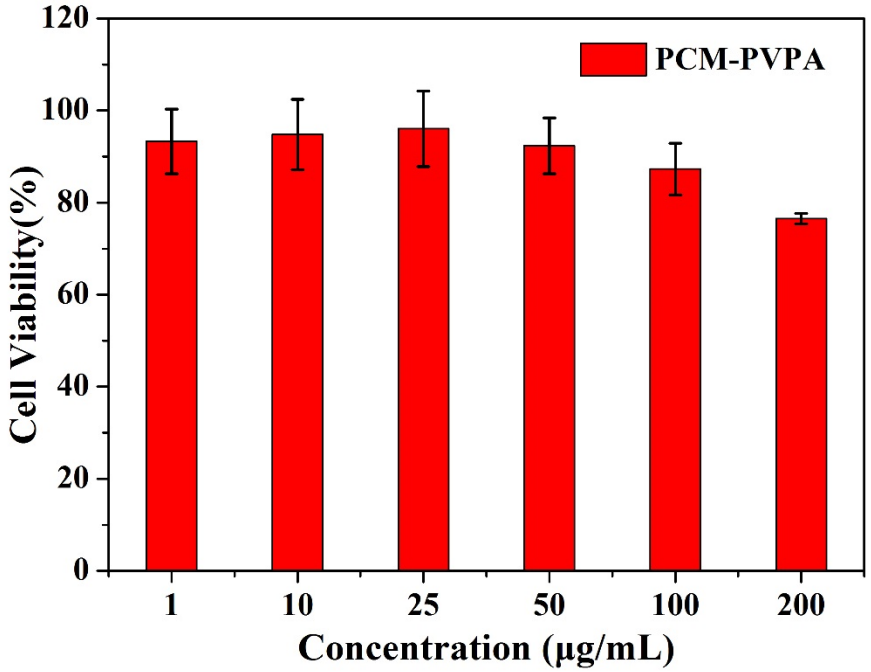

Figure S20. The *in vitro* SH-SY5Y cell viability after treated with PCM-PVAP pseudo block polymer at 37 ^{o}C for 48 h on different polymer concentration.

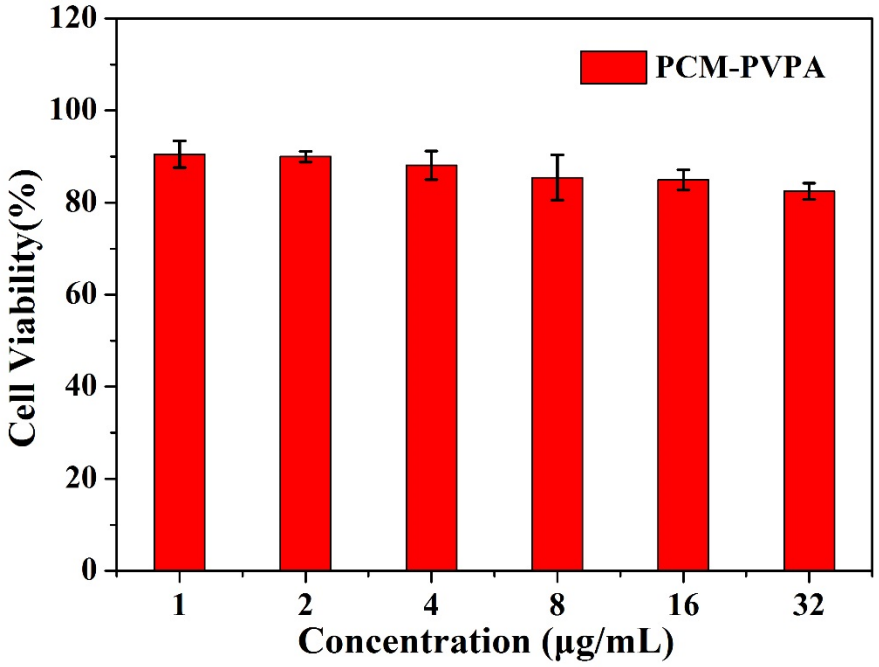

Figure S21. The *in vitro* H22 cell viability after treated with PCM-PVAP pseudo block polymer at 37 ^{o}C for 48 h on different polymer concentration.

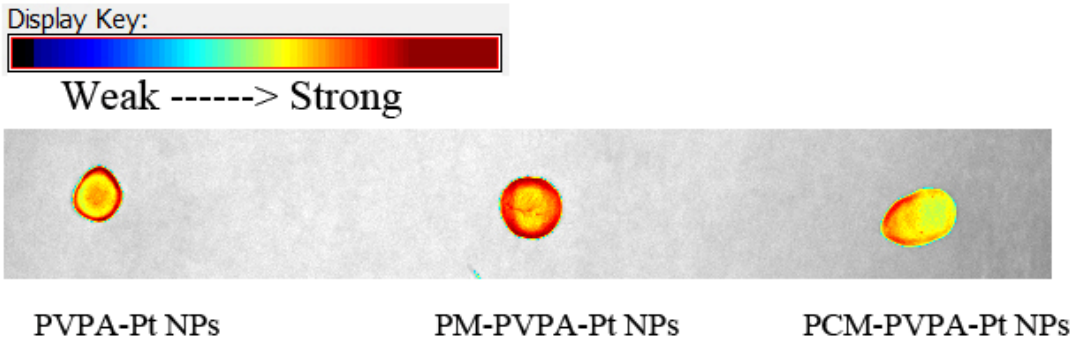

Figure S22. The NIRF images of same amount of NIR797-labeled nanoparticles.

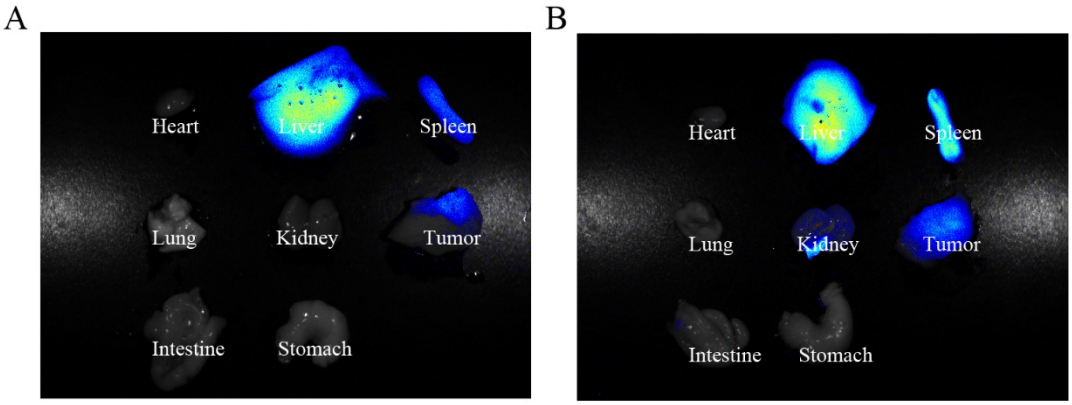

Figure S23. The NIRF images of the tumor and major organs from the mice treated with NIR797-labeled PVPA-Pt NPs (A) and PM-PVPA-Pt NPs (B) after the experiment.

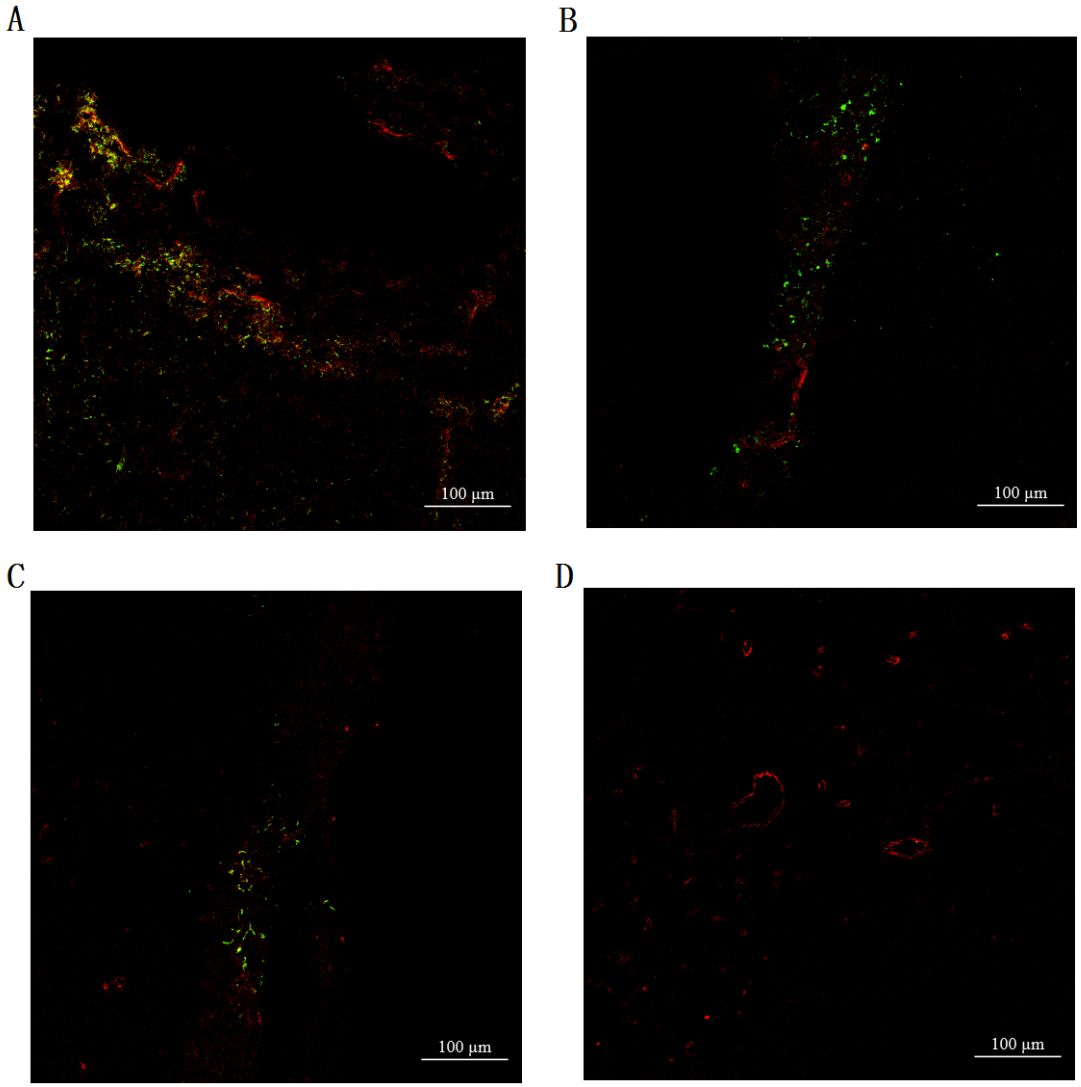

Figure S24. The CLSM images of H22-tumor tissues from the mice treated with FITC-labeled PCM-PVPA-Pt NPs for 12 h (A), 24 h (B), PM-PVPA-Pt NPs for 24 h (C), and PVPA-Pt NPs for 24 h (D).

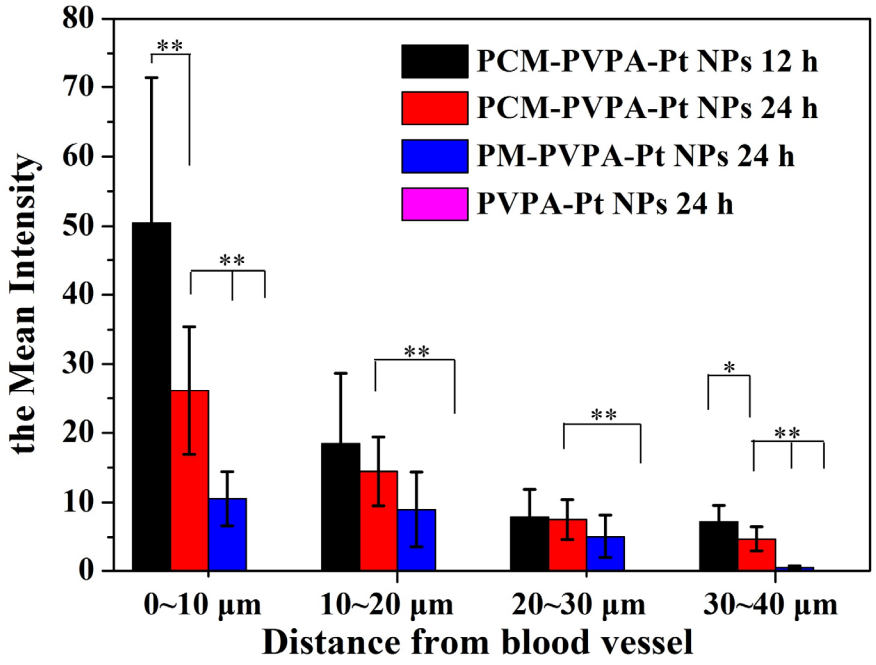

Figure S25. Quantitative relative intensity of these platinum-incorporating nanoparticles with distance from blood vessels. (about ten CLSM images were chosen for the quantitation of each formation, * represents $P < 0.05$, ** represents $P < 0.01$)